

Studies on structural and electrical properties of transition metal ions (Mn, Co and Cu) co-doped $\text{Bi}_{0.9}\text{Dy}_{0.1}\text{FeO}_3$ thin films

C. M. Raghavan · J. W. Kim · S. S. Kim

Received: 5 March 2013 / Accepted: 28 June 2013 / Published online: 9 July 2013
© Springer Science+Business Media New York 2013

Abstract Effects of rare earth Dy and transition metal ($TM = \text{Cu}, \text{Co}$ and Mn) ions co-doping on the structural, electrical and ferroelectric properties of the BiFeO_3 thin films prepared on $\text{Pt}(111)/\text{Ti}/\text{SiO}_2/\text{Si}(100)$ substrates by using a chemical solution deposition method were investigated. All thin films formed as randomly oriented polycrystalline, with no detectable impurity or secondary phases. Among the thin films, the $(\text{Bi}_{0.9}\text{Dy}_{0.1})(\text{Fe}_{0.975}\text{Mn}_{0.025})\text{O}_3$ thin film exhibited well saturated hysteresis loops with remnant polarization ($2P_r$) of $51 \mu\text{C}/\text{cm}^2$ and low coercive electric field ($2E_c$) of 685 at 935 kV/cm and low leakage current density of $1.4 \times 10^{-5} \text{ A}/\text{cm}^2$ at 100 kV/cm. The enhanced properties observed in the co-doped thin films could be considered as being the results of the suppression of ionic defects and of the modified microstructure.

Keywords BiFeO_3 · Thin films · Chemical solution deposition · Electrical properties · Hysteresis loops

1 Introduction

Bismuth ferrite (BiFeO_3 ; BFO) is one of the potential single phase multiferroic compounds in which ferroelectricity and magnetism coexist at room temperature. Both its magnetic and ferroelectric transition temperatures are relatively high (643 and 1,100 K, respectively) [1]. BFO has been synthesized in bulk and thin film forms. However, in thin film form BFO exhibits superior ferroelectric properties due to small lattice strain [2]. BFO is proposed as an active alternative for

the toxic lead zirconium titanate in ferroelectric devices owing to its large polarization [3, 4]. Recent years, considerable attention has been paid to this material because of its fundamental coupling phenomena of the multiple order parameters. Though, BFO showed superior ferroelectric properties, low resistivity due to large electrical leakage, high coercive field and poor hysteresis are considered as major obstacles for the fabrication of practical devices [5–7].

A more active way to improve electrical and ferroelectric properties relies on substituting different ions into the A-site or B-site of the perovskite BFO [8]. In general, doping of rare earth ($RE = \text{La}, \text{Gd}, \text{Eu}, \text{Nd}$ and Tb , etc.) ions to the Bi-site and transition metal ($TM = \text{Co}, \text{Ni}, \text{Cu}, \text{Mn}, \text{Cr}, \text{Mo}$, and Ti , etc.) ions to the Fe-site was strongly recommended to reduce the leakage current density and to improve the ferroelectric properties [8–13]. The rare earth ions doping into BFO stabilizes the perovskite structure by controlling Bi evaporation [14]. According to the literature, the conduction band of BFO is related to the d orbital electronic state of the Fe^{3+} ion, the Fe-site doping by transition metal ions can have a strong influence on physical properties by changing the electronic structure [7]. Doping of the transition metal ions also controls $\text{Fe}^{2+}/\text{Fe}^{3+}$ valence fluctuation through charge compensation [12].

It has been reported that Bi-site substitutions by rare earth ions with smaller ionic radius would induce more buckling in the Fe–O–Fe bond angle accompanying a smaller tolerance factor leading to a more insulating character [8]. The ionic radius of Dy (1.25 Å) with the co-ordination number of twelve is much smaller than that of Bi (1.36 Å), therefore, it can be easily substitute to the Bi-site of BFO. Substitution of the Dy^{3+} is expected to the large structural distortion [15].

In this study, pure BiFeO_3 and co-doped $(\text{Bi}_{0.9}\text{Dy}_{0.1})(\text{Fe}_{0.975}\text{TM}_{0.025})\text{O}_{3\pm\delta}$ ($TM = \text{Mn}, \text{Co}$ and Cu) thin films

C. M. Raghavan · J. W. Kim · S. S. Kim (✉)
Department of Physics, Changwon National University,
Changwon, Gyeongsang 641-773, Republic of Korea
e-mail: sskim@changwon.ac.kr

were prepared on Pt(111)/Ti/SiO₂/Si(100) substrates by using a chemical solution deposition method. The doping effects on the microstructures of the co-doped thin films were investigated by using X-ray diffraction patterns, Raman spectra and scanning electron microscopy. The electrical and the ferroelectric properties for the co-doped thin films were also investigated and the results are discussed in detail.

2 Experimental details

The starting materials used for the precursor solutions were bismuth nitrate pentahydrate (Bi(NO₃)₃·5H₂O), iron nitrate nonahydrate (Fe(NO₃)₃·9H₂O), dysprosium nitrate hexahydrate (Dy(NO₃)₃·6H₂O), manganese nitrate hydrate (Mn(NO₃)₂·xH₂O), cobalt nitrate hexahydrate (Co(NO₃)₃·6H₂O) and copper nitrate hemihydrate (Cu(NO₃)₂·2.5H₂O). Ethylene glycol (6 mL) and 2-methoxyethanol (4 mL) were mixed together by constant stirring at 40 °C in a water bath for 30 min and used as a solvent. Bismuth nitrate pentahydrate (1.5280 g) (5 mol % excess) was added to the mixed solvent and stirred for 30 min. To the above Bi-solution acetic acid (2 mL) was added to catalyze the reaction and stirred for 30 min. Finally, iron nitrate nonahydrate (1.2120 g) was added to form the BFO precursor solution. The resulting solution was subjected to continuous stirring for 3 h at room temperature. For the doping experiments, a measured quantity of dysprosium nitrate hexahydrate (0.1316 g) was added to the Bi-solution containing bismuth nitrate pentahydrate (1.3752 g), transition metal nitrate (manganese nitrate hydrate 0.0134 g, cobalt nitrate hexahydrate 0.0218 g and copper nitrate hemihydrate 0.0174 g) was added to the Bi–Dy solution, separately and stirred for 30 min in turn. Finally, iron nitrate nonahydrate (1.1817 g) was added. The resulting mixture was stirred for 3 h at room temperature. The concentrations of all final solutions were adjusted to 0.1 M.

All thin films were deposited on Pt(111)/Ti/SiO₂/Si(100) substrates by using a spin coating method at a constant spinning rate of 3,000 rpm for 20 s. After spin coating, the wet thin films were prebaked at 360 °C for 10 min on a hot plate. The coating and the prebaking were repeated 12 times to obtain the desired film thickness. Finally, all thin films were subjected to conventional annealing at 550 °C for 30 min under a nitrogen atmosphere for crystallization. Platinum (Pt) electrodes with areas of 1.54×10^{-4} cm² were deposited on the top surface of the thin films by ion sputtering through a metal shadow mask to form a capacitor structure.

The structures of the thin films were investigated by using an X-ray diffractometer (Rigaku, MiniFlex II) and a Raman spectroscopy (Jasco, NRS-3100). Surface morphologies and

film thicknesses were analyzed by using a field emission scanning electron microscope (Tescan, MIRA II LMH). The ferroelectric hysteresis loops of the thin films were measured at a frequency of 10 kHz with triangular pulses by using a standardized ferroelectric test system (Modified Sawyer–Tower circuit with oscilloscope). The leakage current densities of the thin films were measured by using an electrometer (Keithley, 6517A).

3 Results and discussion

The X-ray diffraction (XRD) patterns of the pure BiFeO₃ (BFO) and the rare earth and transition metal co-doped (Bi_{0.9}Dy_{0.1})(Fe_{0.975}TM_{0.025})O_{3±δ} (TM = Mn, Co and Cu, represented as BDFMn, BDFCo and BDFCu) thin films deposited on Pt(111)/Ti/SiO₂/Si(100) substrates are shown in Fig. 1a. All diffraction peaks of the thin films were indexed with reference to the perovskite BFO structure [JCPDS No. 72-2035]. From the XRD analysis, for all thin films, randomly oriented polycrystalline distorted rhombohedral perovskite structure has been observed. Absence of additional/secondary peaks in the diffraction patterns of the co-doped thin films confirms that dopants concentration below the solubility limit of the BFO. From the magnified XRD patterns (Fig. 1b, c), the mild higher angle shifts in the peak positions at the 2θ values of 22.5° (100) and 32° (100)/(11̄0) were observed for the co-doped thin films. This indicates small changes in the lattice parameters of the co-doped thin films. In addition, the diffraction peaks corresponding to (100)/(11̄0) planes were clearly separated for the pure BFO thin film while the peaks were appeared as broad in the co-doped thin films (Fig. 1c). However, we

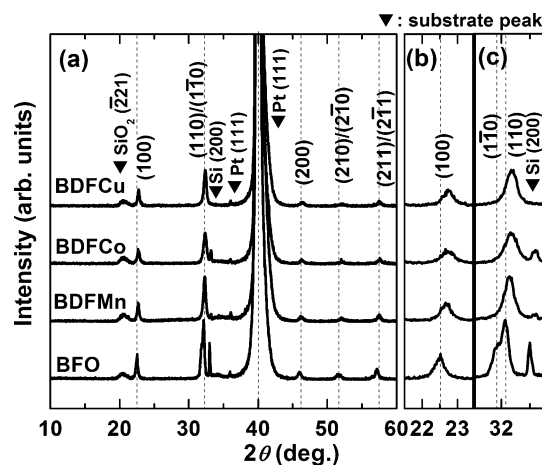


Fig. 1 a XRD patterns of the BFO, BDFMn, BDFCo and BDFCu thin films deposited on Pt(111)/Ti/SiO₂/Si(100) substrates. Magnified XRD patterns in the vicinities of b $2\theta = 22.5^\circ$ and c $2\theta = 32.0^\circ$ to show the lattice distortion in the co-doped thin films

believed that all the thin films show the rhombohedral symmetry without changing the original crystal structure. The small changes in lattice parameters and the peak broadening imply distortion in the rhombohedral lattice due to the incorporation of co-doping elements [16]. The internal stress induced by the chemical substitution leads small distortion in the crystalline lattices of (Dy, TM) co-doped BFO thin films [8, 16]. Recently, Barrionuevo et al. [17] reported the internal stress induced in the Co doped BFO thin film without any structural transformation. Similarly, Singh et al. [18] reported the distortion in the rare earth (La) and transition metal (Mn) ions co-doped BFO thin films. According to Huang et al. [19], the Mn doped BFO thin film keeps a single phase as the Mn content increases up to 15 %. The distortion in perovskite BFO due to internal stress induced by the co-doping elements has significant influence on the ferroelectric properties [16, 17].

The Raman scattering spectra for the pure BFO and the (Dy, TM) co-doped BFO thin films measured at room temperature are shown in Fig. 2. By fitting the measured spectra and decomposing the fitted curves into individual Lorentz components, the exact peak positions have been obtained. According to the group theory, there are 13 ($4A_1 + 9E$) active modes predicted for the rhombohedrally distorted space group $R3c$ [1, 20]. All of the Raman modes observed in the pure BFO and the co-doped thin films are in good agreement with those for the rhombohedrally distorted ($R3c$) perovskite structure. The Raman modes observed in the low frequency A_1 modes are attributed to the Bi–O vibration and the high frequency E modes are related to the Fe–O vibration [21]. The ionic radius of the Dy^{3+} (1.25 Å) with twelve coordination is smaller than that

of the Bi^{3+} (1.45 Å). Hence, the rare earth Dy can readily substitute into the Bi site. As shown in Fig. 2, for the co-doped thin film, the changes in peak intensity and the peak broadening were observed at low frequencies. These are attributed to the dispersion of the Bi–O bonding by doping of rare earth Dy^{3+} ion for Bi sites [22]. The Dy substitution leads to the local disorder in the Bi–O bonding, which in turn broadened the low frequency A_1 modes of the co-doped BFO [22]. Since the concentrations of the transition metal ions are relatively low, they show less significant on the Raman modes of the perovskite BFO in the high frequency region. However, the appearance of intense Raman peak at 621 cm^{-1} for the BDFCu and the BDFMn thin films implies the formation of deformed $[(Fe, Cu)O_6]$ and $[(Fe, Mn)O_6]$ octahedra through Jahn–Teller (J–T) effect [23–25]. The J–T effect describes the geometrical deformation, which often occurs in the transition metal ions within octahedral configuration [26]. In general, the J–T effect pronounces with the transition metal ions having d^9 and d^4 electronic configuration under rare earth environment [25, 26]. Hence, substitution of Mn^{3+} (d^4 electronic state) and Cu^{2+} (d^9 electronic state) into the Fe site of the BFO leads more geometrical deformation in the perovskite oxygen octahedron through J–T effect [23, 24]. The small shifts in the peak positions at high frequencies for the co-doped thin films might be related to the transition metal ion dopants on the Fe-site of the BFO. All the Raman active modes for the pure and the co-doped thin films are given in Table 1.

The surface morphologies and the cross-sectional micrographs of the BFO, BDFMn, BDFCo and BDFCu thin films are shown in Fig. 3. The difference in surface morphologies of the co-doped thin films compared to the pure BFO clearly implies that influence of rare earth and transition metal ions on the nucleation of BFO. From the top view of the SEM images, larger grains were observed in the pure BFO. In the case of the co-doped thin films, the smaller grains were aggregated as large grains-cluster. Both rare earth and transition metal ions act as heterogeneous nucleation centers for the perovskite structure, which in turn influence grains and facilitates aggregation [27]. The thicknesses of the thin films

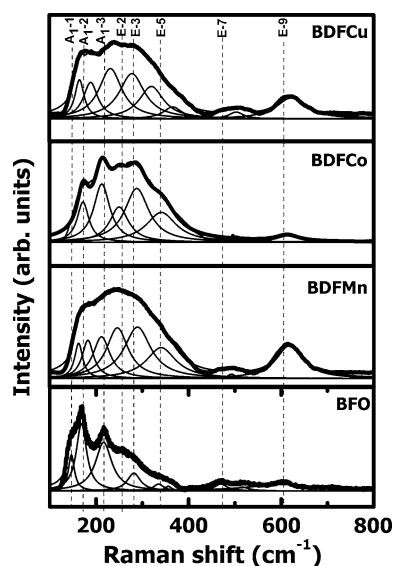
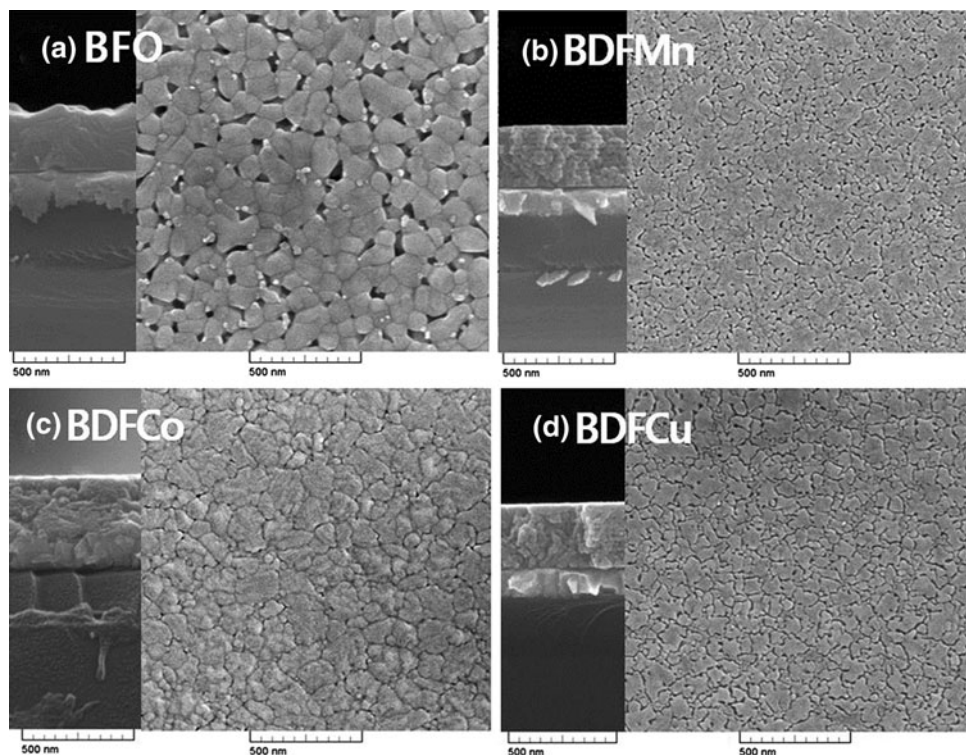


Fig. 2 Raman scattering spectra with decomposed active modes of the BFO, BDFMn, BDFCo and BDFCu thin films

Table 1 Assignment and comparison of the observed Raman frequencies of the BFO, BDFMn, BDFCo and BDFCu thin films

	A_1-1	A_1-2	A_1-3	$E-2$	$E-3$	$E-5$	$E-7$	$E-9$
Assigned Raman modes (cm^{-1})								
BFO	149	168	216	256	283	333	471	602
BDFMn	–	162	210	248	288	334	485	621
BDFCo	–	170	213	248	290	345	–	608
BDFCu	–	164	–	234	285	335	493	617

Fig. 3 SEM morphologies of the BFO, BDFMn, BDFCo and BDFCu thin films with cross-sectional micrographs



measured from the SEM cross-sectional micrographs were approximately 300 nm (BFO) and 400 nm (BDFMn, BDFCo and BDFCu), respectively.

Figure 4a shows variation of leakage current density (J) as a function of an applied electric field (E) for the pure and the co-doped thin films. The measured leakage current densities of the BFO, BDFMn, BDFCo and BDFCu were 2.5×10^{-2} , 1.4×10^{-5} , 2.7×10^{-5} and 1.2×10^{-4} A/cm², respectively at an applied electric field of 100 kV/cm. The measured leakage current densities of the BDFMn and the BDFCo are three orders lower than that of the BFO thin film. The decrease of leakage current density in the co-doped thin film is mainly attributed to the effective reduction of the defect carriers through charge compensation [28]. Additions of rare earth elements are reported to stabilize the perovskite structure by controlling Bi evaporation and oxygen vacancy formation [14]. Furthermore, the small ionic radius of the Dy induces more buckling in the Fe–O–Fe bond angle accompanying a smaller tolerance factor leading to a more insulating character [8]. Co-doping of transition metal ion controls the Fe²⁺/Fe³⁺ charge fluctuation in perovskite BFO and further reduces the leakage current density. Among the thin films, the BDFMn thin film showed the lowest leakage current density, which might be attributed to the more changes in the [FeO₆] octahedra through J–T effect. Presence of Fe and Mn in the same lattice [(Fe, Mn)O₆] leads more tilting in the perovskite octahedra under rare earth environment [29, 30]. These crystallographic changes observed in the BDFMn thin film have strong influence on the electrical and the ferroelectric

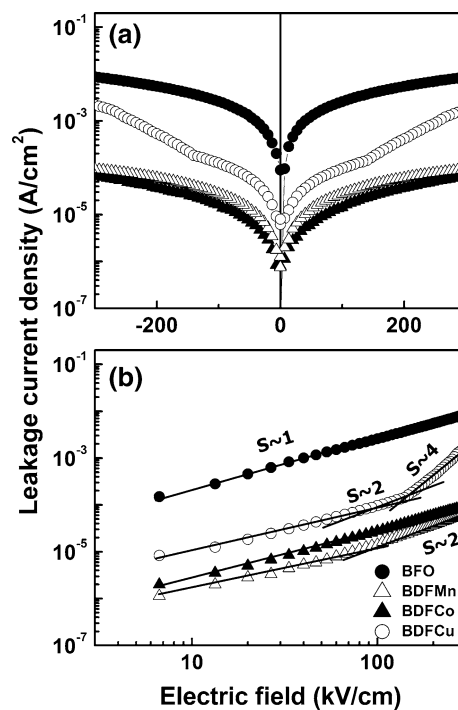


Fig. 4 a Leakage current densities of the BFO, BDFMn, BDFCo and BDFCu thin films and b $\log(J)$ – $\log(E)$ characteristics of the thin films

properties [31]. Furthermore, substitution of the Mn³⁺ for Fe³⁺ maintains charge neutrality in the perovskite BFO structure. The leakage current densities of the BDFMn and the BDFCo thin films were found to be same order. The dense

microstructure with large grains leads improved electrical properties in the BDFCo thin film compared to the BDFCu thin film. However, the J value of the BDFCu was found to be two orders lower than that of the pure BFO, which indicates an effective reduction of oxygen vacancies through charge compensation by Dy and Cu ions [28].

The conduction mechanisms for the leakage current densities observed in the pure BFO and the co-doped thin films were studied by logarithmic plots of the leakage current density versus applied electric field ($\log(J)$ – $\log(E)$) as shown in Fig. 4b. The linearity of the lines with respect to applied electric field for the pure and the BDFCo thin films with the slope (S) value ~ 1.0 indicates Ohmic conduction mechanism and is dominated by thermally stimulated free electrons [32]. The leakage current for Ohmic conduction can be expressed as [32]

$$J = e\mu N_e E,$$

where e is the electron charge, μ is the free carrier mobility, N_e is the density of the thermally stimulated electrons and E is the applied electric field.

At low electric field region, both the BDFMn and the BDFCu showed Ohmic conduction mechanism. However, the change of the slope value from $S \sim 1$ to $S \sim 2$ with an increase of applied electric field for the thin films implies the change of conduction mechanism from Ohmic to space charge limited (SCL) conduction [32, 33]. With an increase of electric field, the density of free electrons due to charge carriers becomes injection larger than the density of thermally stimulated electrons [32]. The current density for SCL conduction is given by [32]

$$J_{\text{SCL}} = \left(\frac{9\mu\epsilon_0\epsilon_r\theta V^2}{8d^3} \right),$$

where V is the applied voltage, ϵ_r is the static dielectric constant, ϵ_0 is the permittivity of free space, d is the thickness of thin film and θ is the ratio of the total density of free electrons to the trapped electrons.

In the case of BDFCu thin film, an abrupt increase of the current with increase of the applied electric field, the slope value changed to greater than 4 indicating the trap filled limited (TFL) conduction mechanism [32]. It implies, at high electric field region, the applied voltage forces all the available traps to become filled and the excess charge carriers lead drastic increase of the current with the large slope value. The voltage at which abrupt increase of the current occurs is TFL voltage and given by [32]

$$V_{\text{TFL}} = \frac{eN_t d^2}{2\epsilon_0\epsilon_r}$$

where N_t is the total trap density. Thus, the leakage current observed in the BDFCu were originated from Ohmic, SCL and TFL conduction mechanisms.

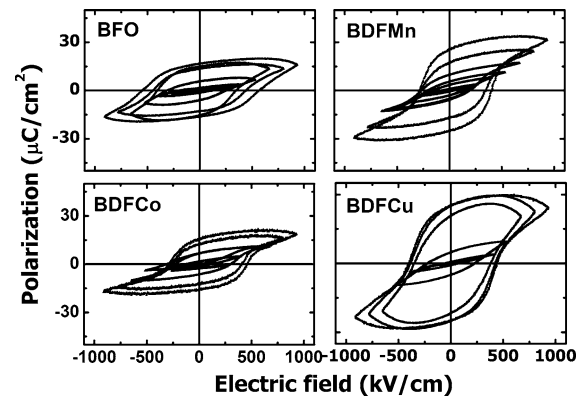


Fig. 5 Ferroelectric P – E hysteresis loops of the BFO, BDFMn, BDFCo and BDFCu thin films

The ferroelectric polarization–electric field (P – E) hysteresis loops of the BFO, BDFMn, BDFCo and BDFCu thin films are shown in Fig. 5. The co-doped thin films showed improved ferroelectric properties compared to the pure BFO thin film. The low remnant polarization ($2P_r$) of $33 \mu\text{C}/\text{cm}^2$ and the large coercive field ($2E_c$) of $1,120 \text{ kV}/\text{cm}$ at an applied electric field of $935 \text{ kV}/\text{cm}$ were observed for the pure BFO thin film. The $2P_r$ and the $2E_c$ values of the BDFMn, BDFCo and BDFCu thin films were $51 \mu\text{C}/\text{cm}^2$ and $685 \text{ kV}/\text{cm}$, $31 \mu\text{C}/\text{cm}^2$ and $738 \text{ kV}/\text{cm}$ and $50 \mu\text{C}/\text{cm}^2$ and $836 \text{ kV}/\text{cm}$ at an applied electric field of $935 \text{ kV}/\text{cm}$, respectively. The measured electrical and ferroelectric properties of the (Dy, TM) co-doped thin films are better than that of Dy- alone doped BFO [34, 35]. Hence, the key role of transition metal ions in the improvement of electrical and ferroelectric properties of BFO thin film clearly inferred. There is a good consistency between the leakage current density and the ferroelectric properties of the thin films. The increase of $2P_r$ and the decrease of $2E_c$ for the co-doped thin films are well correlated with the low leakage current density compared to the pure BFO thin film. In addition to this, the lattice distortions due to the internal stress induced by the co-doping elements also enhance ferroelectric polarization [17, 18]. Among the thin films, the BDFMn thin film shows better ferroelectric properties than other thin films. The large polarization and the low coercive field observed in the BDFMn thin film are attributed to the low leakage current density and the formation of highly deformed $[(\text{Fe}, \text{Mn})\text{O}_6]$ octahedra with distorted perovskite structure [31–36]. While the BDFCu thin film shows relatively large leakage current density compared to the BDFMn and the BDFCo thin films, hence it exhibits a poor hysteresis behavior.

In overall consideration, control of oxygen vacancies, charge fluctuation, changes in microstructure and internal stress due to the lattice distortion by the co-doping elements lead significant improvements in the electrical and ferroelectric properties of the perovskite BFO.

4 Conclusions

Effects of (Dy, *TM*) (*TM* = Mn, Co and Cu) co-doping on the structural, electrical and ferroelectric properties of the BFO thin films prepared on Pt(111)/Ti/SiO₂/Si(100) substrates via a chemical solution deposition were investigated. The distorted rhombohedral perovskite structures for the pure BFO and the co-doped thin films were confirmed by using an XRD and a Raman scattering analysis. Significant improvements, such as reduced leakage current density and coercive field, were observed for the (Dy, Mn) co-doped BFO thin film. The enhanced electrical and ferroelectric properties in the BDFMn thin film could be explained by the combined effects of reduced oxygen vacancies, internal stress more deformation of [(Fe, Mn)O₆] octahedra and changes in microstructural features.

Acknowledgments This work was supported by Priority Research Centers Program through the National Research Foundation of Korea (NRF) funded by the Ministry of Education, Science and Technology (2010-0029634).

References

- Singh MK, Jang HM, Ryu S, Jo MH (2006) Appl Phys Lett 88:042907
- Neaton JB, Ederer C, Waghmare UV, Spaldin NA, Rabe KM (2005) Phys Rev B 71:014113
- Ishiwara H (2012) Curr Appl Phys 12:603–611
- Chu YH, Zhan Q, Martin LW, Cruz MP, Yang PL, Pabst GW, Zavaliche F, Yang SY, Zhang JX, Chen LQ, Schlom DG, Lin IN, Wu TB, Ramesh R (2006) Adv Mater 18:2307–2311
- Palkar VR, John J, Pinto R (2002) Appl Phys Lett 80:1628–1630
- Singh SK, Ishiwara H, Maruyama K (2006) J Appl Phys 100:064102
- Casper MD, Losego MD, Maria JP (2013) J Mater Sci 48:1578–1584
- Yang CH, Kan D, Takeuchi I, Nagarajan V, Seidel J (2012) Phys Chem Chem Phys 14:15953–15962
- Simões AZ, Cavalcante LS, Moura F, Longo E, Varela JA (2011) J Alloy Compd 509:5326–5335
- Yu B, Li M, Hu Z, Pei L, Guo D, Zhao X, Dong S (2008) Appl Phys Lett 93:182909
- Uniyal P, Yadav KL (2009) J Phys: Condens Matter 21:405901
- Wang X, Liu H, Yan B (2009) J Eur Ceram Soc 29:1183–1187
- Naganuma H, Miura J, Okamura S (2008) Appl Phys Lett 93:052901
- Ke Q, Lou X, Wang Y, Wang J (2010) Phys Rev B 82:024102
- Wang Y, Nan CW (2008) J Appl Phys 103:024103
- Yan F, Lai MO, Lu L, Zhu TJ (2010) J Phys Chem C 114:6994–6998
- Barrionuevo DG, Singh SP, Katiyar RS, Tomar MS (2010) MRS Proc 1256, 1256-N06-47. doi:10.1557/PROC-1256-N06-47
- Singh SK, Maruyama K, Ishiwara H (2007) Appl Phys Lett 91:112913
- Huang JZ, Wang Y, Lin Y, Li M, Nan CW (2009) J Appl Phys 106:063911
- Kothari D, Reddy VR, Sathe VG, Gupta A, Banerjee A, Awasthi AM (2008) J Magn Magn Mater 320:548–552
- Hermet P, Goffinet M, Kreisel J, Ghosez Ph (2007) Phys Rev B 75:220102
- Yuan GL, Or SW, Chan HLW, Liu ZG (2007) J Appl Phys 101:024106
- Lahmar A, Habouti S, Dietze M, Solterbeck C-H, Souni ME (2009) Appl Phys Lett 94:012903
- Kartopu G, Lahmar A, Habouti S, Solterbeck C-L, Elouadi B, Souni ME (2008) Appl Phys Lett 92:151910
- Martín-Carrón L, de Andrés A, Martínez-Lope MJ, Casais MT, Alonso JA (2002) Phys Rev B 66:174303
- Shriver, DF, Atkins, PW (1999) Inorganic chemistry, 3rd edn. Oxford University Press, Oxford, pp 235–236. ISBN 0-19-850330-X
- Chung CF, Lin JP, Wu JM (2006) Appl Phys Lett 88:242909
- Qi X, Dho J, Tomov R, Blamire MG, Driscoll JLM (2005) Appl Phys Lett 86:062903
- Pradhan DK, Choudhary RNP, Rinaldi C, Katiyar RS (2009) J Appl Phys 106:024102
- Bridges CA, Sefat AS, Payzant EA, Cranswick L, Paranthaman MP (2011) J Solid State Chem 184:830–842
- Lahmar A, Habouti S, Solterbeck CH, Souni ME, Elouadi B (2009) J Appl Phys 105:014111
- Wang C, Takahashi M, Fujino H, Zhao X, Kume E, Horiuchi T, Sakai S (2006) J Appl Phys 99:054104
- Lampert MA (1956) Phys Rev 103:1648–1656
- Li Y, Yu J, Li J, Zheng C, Wu Y, Zhao Y, Wang M, Wang Y (2011) J Mater Sci: Mater Electron 22:323–327
- Zhang S, Luo W, Wang L, Wang D, Ma Y (2010) J Appl Phys 107:054110
- Huang JZ, Shen Y, Li M, Nan CW (2011) J Appl Phys 110:094106